


Insights into catalytic activity and selectivity of 5-Hydroxymethylfurfural oxidation on gold single-crystal electrodes

Received: 21 October 2024

Accepted: 28 March 2025

Published online: 09 April 2025

 Check for updatesLorena Chico-Mesa, Antonio Rodes, Rosa M. Arán-Ais  & Enrique Herrero 

The selective electrochemical oxidation of 5-hydroxymethylfurfural (HMF) to 2,5-furandicarboxylic acid (FDCA) holds transformative potential for advancing sustainable, bio-based polymer production. In this study, we unveil the pivotal role of gold single-crystal electrode surface orientation in directing HMF oxidation pathways under alkaline conditions. Using cyclic voltammetry, we systematically evaluate the oxidation behavior on Au(111), Au(100), Au(110), Au(311), Au(331), and Au(210) surfaces. Our findings reveal that Au(111) and Au(100) surfaces exhibit superior catalytic activity for the complete oxidation to FDCA, while Au(110) promotes the selective formation of 5-hydroxymethyl-2-furancarboxylic acid (HMFA). These differences in activity are closely linked to the crystallographic structure, influencing adsorption energies and reaction intermediates. In situ infrared reflection absorption spectroscopy (IRRAS) and attenuated total reflectance (ATR) spectroscopy provide direct molecular insights, identifying distinct vibrational signatures of intermediates and products. This study highlights the critical role of electrode surface structure in tuning reaction efficiency and selectivity, contributing to the development of more efficient catalytic processes in green chemistry.

The growing concerns regarding the depletion of fossil fuels and the accompanying environmental issues, such as air pollution and global warming, highlight the urgent need for a shift towards a sustainable energy future. In this context, the catalytic conversion of biomass into fuels and chemicals using electricity from renewable energy sources appears particularly promising¹. Biomass and its derivatives, being some of the most abundant hydrocarbon resources, provide a nearly unlimited supply of feedstocks. One of the most notable processes in this area is the electrochemical oxidation of biomass, specifically the transformation of 5-hydroxymethylfurfural (HMF) into 2,5-furandicarboxylic acid (FDCA)^{2–5}. FDCA is especially important because it is a precursor to polyethylene furanoate (PEF), a bio-based polymer that is non-toxic, renewable, and recyclable. It displays comparable properties to traditional plastics and has the potential to replace polyethylene terephthalate (PET), an oil-based polymer, in various applications, underscoring its significance in sustainable material science.

The scheme in Fig. 1 illustrates the oxidation pathways of HMF to FDCA through a series of oxidation steps involving both the aldehyde and alcohol functional groups. The mechanism contains two possible paths. Initially, the alcohol group of HMF can be oxidized to an aldehyde group yielding 2,5-diformylfuran (DFF) or, alternatively, the aldehyde group can be oxidized to produce 5-hydroxymethyl-2-furancarboxylic acid (HMFA). Subsequently, the oxidation of an aldehyde group in DFF or an alcohol group in HMFA leads to the formation of 5-formyl-2-furancarboxylic acid (FFCA). Finally, the oxidation of the aldehyde group in FFCA results in the formation of FDCA. Previous studies conducted with gold electrodes in alkaline media have demonstrated that the oxidation pathway predominantly proceeds through the formation of HMFA⁶.

The oxidation of HMF has been extensively studied using non-noble metal catalysts such as nickel^{2,3,5,7,8} and copper-based^{8,9} catalysts. While these systems offer clear advantages in terms of cost and abundance, single-crystal electrodes are ideal for investigating the

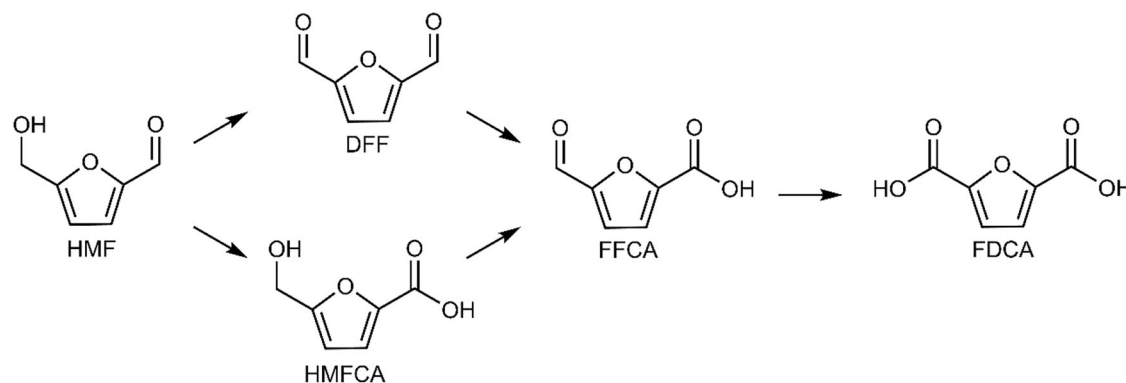


Fig. 1 | Schematic overview of the key reaction intermediates leading to FDCA. Two oxidation pathways from HMF are shown, proceeding through either DFF or HMFCa, and ultimately converging at FFCA to yield FDCA.

dependence of the reaction on surface structure. However, the methods for preparing single-crystal electrodes of non-noble metals are not as advanced, and these single-crystals are not nearly as well-characterized in the literature. Gold, on the other hand, not only demonstrates exceptional catalytic activity towards HMF oxidation but also provides single-crystal surfaces that are deeply characterized in published research. Recent studies have highlighted the efficiency of gold electrodes in catalyzing the oxidation of HMF to FDCA with lower overpotentials than non-noble metal catalysts^{10–12}. These investigations have demonstrated that the predominant reaction product when using gold as an electrode in alkaline media is HMFCa, with selectivity exceeding 90%, while FDCA is produced at higher potentials but with lower yields. Despite this findings, most published studies in this field have focused on nanoparticle catalysis, and a deeper understanding of the reaction's dependence on surface structure is still needed. In this context, employing gold single-crystal electrodes offers a promising approach. The well-defined surfaces with known crystallographic orientations provided by gold single-crystal electrodes enable detailed studies of the structure–reactivity relationships in HMF oxidation.

Additionally, it is well-documented that the oxidation reactions on gold electrocatalysts are highly dependent on the pH of the electrolyte¹³. In the case of HMF, alkaline conditions favor the formation of FDCA. However, the exact reaction mechanism remains a subject of debate. Some studies propose that HMF adsorbs onto the electrode surface via the aromatic ring¹⁴, while others suggest that the molecule adsorbs through the aldehyde group¹⁵. More specifically, it has been suggested that HMF undergoes adsorption via a gem-diol structure, facilitating subsequent oxidation steps. Understanding these adsorption behaviors is crucial, as they directly influence the reaction pathways and the efficiency of the electrochemical oxidation process.

At pH 13, the production of FDCA from the oxidation of HMF is favored, making it an interesting media for studying this reaction. In addition, recent studies point out the convenience of coupling HMF oxidation with water splitting in an alkaline electrolyzer, since it allows for simultaneous H₂ and FDCA production at a lower energy cost compared to traditional water electrolysis^{16,17}. However, the stability of HMF in alkaline media is critically influenced by pH. At pH 13, HMF tends to degrade rapidly into humins, which are non-oxidizable polymeric species¹⁸. Nonetheless, the presence of strong alkaline conditions also facilitates the Cannizzaro reaction, leading to the formation of more stable intermediates such as HMFCa and 2,5-dihydroxymethylfuran (DHMF). These intermediates can be further oxidized to FDCA, thus enabling the indirect oxidation of HMF at high potentials and alkaline concentrations while minimizing humin formation¹⁹.

To further investigate the electrochemical oxidation of HMF, in this study gold single-crystal electrodes are employed at different pH values. These electrodes are chosen due to their well-defined surface

orientations, which allow for a detailed study of the oxidation mechanisms at a molecular level. Experiments are conducted in alkaline media to facilitate the oxidation process, with particular attention given to the pH-dependent behavior of the reaction. Additionally, infrared reflection absorption spectroscopy (IRRAS) experiments are conducted to in situ identify the reaction intermediates and products. The primary focus is to understand how the surface orientation of the electrodes influences the electro-oxidation pathways of HMF, as this provides both practical insights into optimizing the conversion of HMF to FDCA and fundamental knowledge on the role of surface structure in the electrochemical oxidation of organic molecules. This dual approach aims to advance the development of more efficient electrocatalysts for biomass conversion and deepen the understanding of surface chemistry in electrocatalytic processes.

Results and discussion

Electrochemical behavior of HMF on gold basal planes

Cyclic voltammograms of Au(100), Au(110), and Au(111) electrodes in 0.1 M NaOH, both in the absence and presence of HMF, are presented in Figs. 2 and S1. The upper potential limit was set at 1.20 V in Fig. 2 to avoid gold oxidation, which not only may induce surface disordering but also hinders HMF oxidation (Fig. S1). This approach ensures that the surface remains ordered throughout the study. The characteristic voltammetric profiles of these electrodes in 0.1 M NaOH agree with those previously reported²⁰, thus confirming that the surfaces are clean and well-ordered.

It is well established that gold electrodes undergo surface reconstruction after a heat treatment. This phenomenon occurs because atoms in the top layer experience different forces than those in the bulk due to the asymmetric environment caused by missing neighbors. Consequently, surface atoms displace laterally, creating more densely packed surfaces compared to the bulk. Flame-annealing before recording the voltammograms induces this effect^{21,22}. The Au(111) surface undergoes reconstruction, forming (22 × √3) and (23 × √3) unit cells, resulting in a compression of the uppermost atomic layer along the [110] direction by 4.20% and 4.55%, respectively (see the hard sphere model in Fig. S2). The reconstructed surface is stable at low potential but above 1.10 V this reconstruction is lifted, as evidenced by the peak at 1.10 V (Fig. 2)²³. Moreover, Au(100) reconstructs into a hexagonal close-packed form, creating the so-called hex structure (Fig. S2), with the lifting of the reconstruction associated with the sharp anodic peak slightly above 1.00 V. In the case of Au(110), the lifting occurs at potentials higher than 0.80 V. For the reconstructed surfaces, the coordination number of Au(110) is about 7, while for Au(111) and Au(100), this value is 9.

The voltammetric profiles in the presence of HMF reported in Fig. 2 show a clear surface structure dependence. For the Au(111), the onset potential for HMF oxidation is ca. 0.30 V, and currents in the

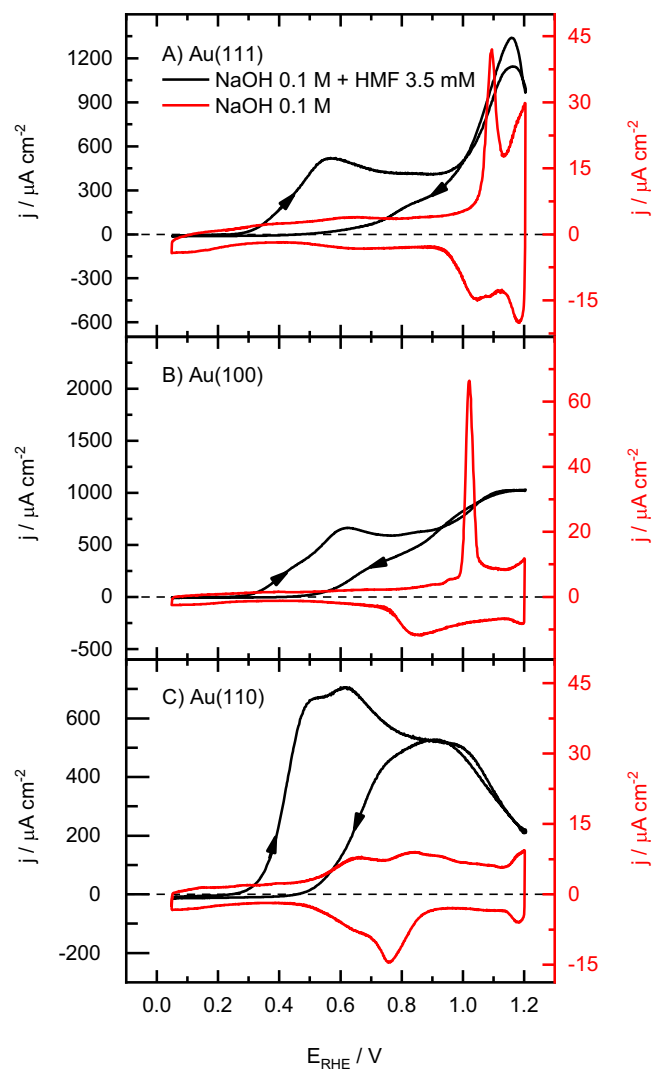


Fig. 2 | Comparative overview of HMF electrooxidation on different Au single-crystal electrodes in alkaline media. Cyclic voltammograms of (A) Au(111), (B) Au(100), and (C) Au(110) in 0.1 M NaOH (red line and right axis), and in 0.1 M NaOH + 3.5 mM HMF (black line and left axis). Arrows of the voltammogram obtained in the HMF solution indicate the scan direction. All curves correspond to the first voltammetric cycle after flame-annealing. Initial potential: 0.10 V. Scan rate: 50 mV·s⁻¹. Source data are provided as a Source Data file.

positive scan direction are larger than those in the negative direction. In the positive scan direction, the profile seems to have two differentiated peaks, one at ca. 0.55 V and a second one, more intense, at 1.15 V. On the other hand, in the negative scan direction, only the process at high potential is observed. For the Au(100) electrode, the overall shape is very similar, although the peaks are less defined and seem to have some shoulders. Besides, for the Au(110) electrode, the second process is very broad and its current intensity has diminished significantly. Additionally, it should be mentioned that the reconstruction peaks seem to be absent in the profiles recorded in the HMF-containing solutions. It is well documented that the specific adsorption of species leads to the lifting of the reconstruction. In this case, the effect of the adsorption of organic molecules on gold surfaces has been extensively studied^{24,25}. It is known that the interaction between the electrode surface and the π electrons of aromatic organic molecules influences the potential stability range of the reconstructed structure. Conversely, previous studies on ethanol oxidation using Au single-crystals demonstrate that the stability of the reconstruction is not affected by the presence of ethanol, as the lifting peak is observed

in the voltammograms without changes in its shape and potential²⁶. Thus, it can be proposed that the interaction of the HMF with the electrode surface lifts the reconstruction.

The differences between the HMF oxidation profiles obtained for low-index electrodes can be better observed in Fig. S3. As can be seen, the onset potential is the same for all the surfaces, although the currents for the process at low potentials are larger for the Au(110) electrode. On the other hand, the second process is much more prominent on the Au(111) electrode. On the Au(110) surface, the oxidation is inhibited at high potentials, coinciding with the onset of the formation of an adsorbed OH layer (see also Fig. S1). This voltammetric behavior described above is compatible with a mechanism in which the oxidation of HMF to FDCA takes place with the formation of at least one intermediate species. The oxidation of this intermediate species is also a structure-sensitive process.

To determine the origin of the large differences between the HMF oxidation currents in both scan directions, several additional experiments were conducted. Whether the formation of strongly adsorbed species is responsible for the hysteresis will be analysed first. For this purpose, five consecutive voltammetric cycles were recorded for each low index plane (Fig. S4). As can be seen, the overall shape of the profile is maintained for each electrode, although the onset potential is displaced to higher values as the number of cycles increases. This shift may indicate that some species (intermediates or products) are being adsorbed on the surface, but their adsorption strength or coverage is not enough to inhibit the reaction. Upon increasing the upper potential up to 1.70 V, the onset shifts back to values closer to that observed in the first cycle, as shown in Fig. S5. These observations may be attributed to the adsorption of a reaction intermediate or/and products on the electrode surface, which desorb when the surface is oxidized. This poisoning preferentially occurs on Au(111) and Au(100) surfaces, as evidenced by the larger displacement of the onset observed for these two surfaces. This is consistent with previous studies on the oxidation of furfural on gold, where it was suggested that the rate-limiting step is the desorption of furoate, the reaction product²⁷. Notably, the only structural difference between HMF and furfural is the presence of the hydroxymethyl group in HMF²⁷. The presence of adsorbed products can potentially block the active sites required for the oxidation of the initial reactant, thereby hindering its oxidation in subsequent cycles. This behavior indicates a competitive interaction between the reactant and the reaction products on the electrode surface, which impacts the efficiency of the electrocatalytic process. This phenomenon suggests that the adsorption of reaction intermediates or products plays a significant role in modulating the electrochemical activity of the electrode, influencing both the onset potential and the overall oxidation kinetics.

Additionally, the differences between both scan directions for each voltammetric cycle in Fig. S4 are still significant, which implies that the adsorption of intermediate species is not the reason for this behavior. Further insight into this response can be gained from the profiles with different upper potential limits (Fig. 3). To prevent any influence from species adsorbed in previous scans, the electrode was freshly annealed before each alteration of the upper limit. As can be seen, when the upper potential limit is below the first peak potential, the positive and negative scan directions overlap. On the other hand, when the upper potential limit is above the first peak but lower than 0.90 V, the shape resembles that of an irreversible oxidation process controlled by diffusion. Finally, for upper potentials above 1.00 V, the differences between the traces recorded in the positive and negative scan directions do not depend anymore on the value of the upper potential. Thus, it can be proposed that, during the first peak, the HMF oxidation leads to the formation of an intermediate species, in a

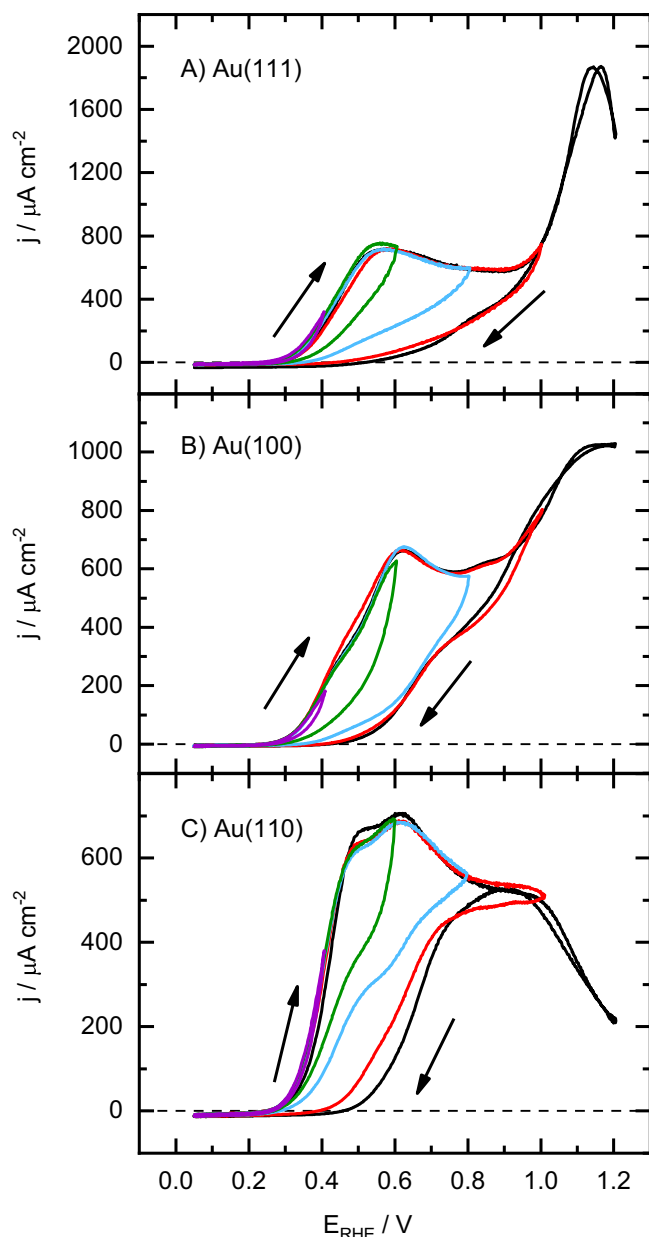


Fig. 3 | Stepwise extension of the potential window to reveal the onset and progression of HMF oxidation at different Au single-crystal electrodes. Cyclic voltammograms of (A) Au(111), (B) Au(100), and (C) Au(110) from 0.05 V to 0.40 V (purple), 0.60 V (green), 0.80 V (blue), 1.00 V (red), and 1.20 V (black) in 3.5 mM HMF + 0.1 M NaOH. Each voltammogram is recorded just after flame-annealing the electrode. Scan rate: 50 mV s⁻¹. Source data are provided as a Source Data file.

process controlled by the kinetics and HMF diffusion to the electrode surface. In contrast, the second process would be related to the oxidation of this intermediate species. These observations are consistent with the results presented in Fig. S6, where cyclic voltammograms recorded at various scan rates show that the current does not increase linearly with scan rate, indicating a mixed-control regime.

HMF oxidation at stepped surfaces

Surfaces with low-coordinated atoms are known to be more reactive²⁸. For this reason, HMF oxidation was also investigated on stepped surfaces. The selected surfaces are those at the so-called turning point of the edges of the stereographic triangle, and contain two atom-wide terraces with one orientation and a monoatomic step with a second basal orientation. The term turning point recalls that, for those surfaces,

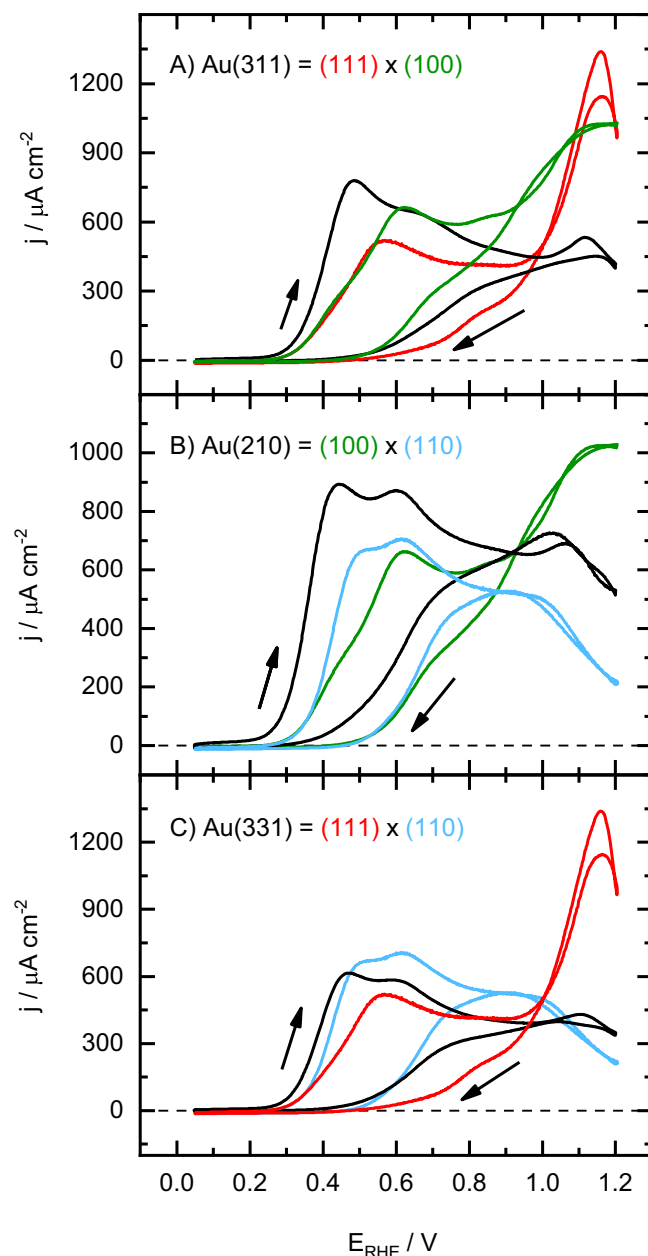


Fig. 4 | Comparative voltammetric behavior of stepped and low-index Au electrodes for HMF electrooxidation in alkaline media. Voltammetric profiles for the oxidation of 3.5 mM HMF in 0.1 M NaOH on (A) Au(311), Au(111), and Au(100); (B) Au(210), Au(100), and Au(110); (C) Au(331), Au(111), and Au(110) electrodes. Stepped surface (black lines), Au(111) (red lines), Au(100) (green lines), and Au(100) (blue lines). Arrows indicate the scan direction. Scan rate: 50 mV s⁻¹. Source data are provided as a Source Data file.

the role of the terrace and step can be exchanged. The studied surfaces are Au(311), Au(210), and Au(331). Figure 4 shows the voltammetric profiles for HMF oxidation of these surfaces and compares them with the two basal orientations in the same zone. The characteristic profiles of these electrodes in 0.1 M NaOH are shown in Fig. S7. In the three cases, the onset potential for the HMF oxidation shifts to lower potential values when compared to the corresponding basal planes, indicating that low coordinated sites are favorable for the initial oxidation of the molecule. In fact, Au(210) exhibits the lowest onset potential, which can be attributed to its high reactivity, as it is the least densely packed single-crystal plane²⁹. It is known from previous studies that the potentials of zero charge (pzc) for various gold surfaces exhibit the following order:

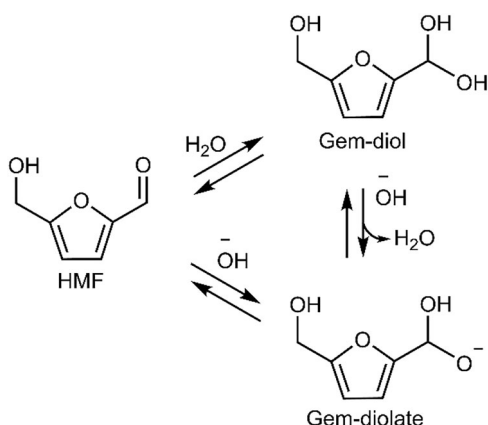


Fig. 5 | Transient species and their interconversions under basic conditions. Schematic representation of the equilibrium reactions involving HMF, the gem-diol, and the gem-diolate species in alkaline conditions.

$\text{Au}(210) > \text{Au}(110) > \text{Au}(311) > \text{Au}(331) > \text{Au}(100) > \text{Au}(111)$ ³⁰. The pzc values indicate the potential at which the surface has a neutral charge, influencing the adsorption and reactivity of species on the electrode surface. At potentials positive to the pzc, the adsorption of negatively charged species such as OH^- is favored. This enhanced adsorption may facilitate the oxidation process, resulting in lower onset potentials for the oxidation reaction. The onset is nearly identical for the different Au basal planes, with distinct behavior among surface orientations emerging only at $E > 0.35$ V. In this lower potentials region, the Au(110) electrode exhibits higher currents for the process. While pzc is an important parameter indicating the potential at which the surface is electrically neutral, the reactivity for oxidation reactions is not solely determined by the surface charge. Other factors, such as adsorption geometry can also play significant roles in dictating the electrochemical behavior of these surfaces. Moreover, the voltammetric curves shown in Fig. 4 indicate that the process at high potential on the stepped surfaces is inhibited when compared to the Au(111) or Au(100) electrodes, implying a distinct surface structure dependence for the two different oxidation steps of the process.

pH effects

The effect of solution pH on the reactivity of HMF can also provide clues to untangle the reaction mechanism. There are several examples in which there is an important relationship between the solution pH and reactivity on gold. This is the case of the oxidation of alcohols and aldehydes. It has been demonstrated that the formation of alkoxide ions, which are more reactive than their parent alcohols, facilitate a higher oxidation activity³¹. This pH-dependent behavior is linked to the base-catalyzed nature of the initial deprotonation step, suggesting a direct correlation between the pK_a of the alcohol and its oxidation efficiency on gold. Additionally, it has been suggested that, at higher pH values, the increased presence of hydroxide ions may modify the electronic structure of gold, lowering the energy barriers for oxidation processes³². This interaction between the gold surface and the hydroxide ions in the solution enhances the selective oxidation capabilities of gold, making it a more effective catalyst in alkaline media. Additionally, it has been suggested that hydroxide ions at higher pH values interact with the aldehyde functional group forming diolate and gem-diol species, accelerating the oxidation process, and stabilizing the resultant oxidized products³³. In this sense, the aldehyde group in HMF is in equilibrium with the gem-diol and diolate forms in alkaline solutions (Fig. 5). HMF undergoes hydration of its aldehyde group in the presence of water to form the gem-diol¹⁵. Under alkaline

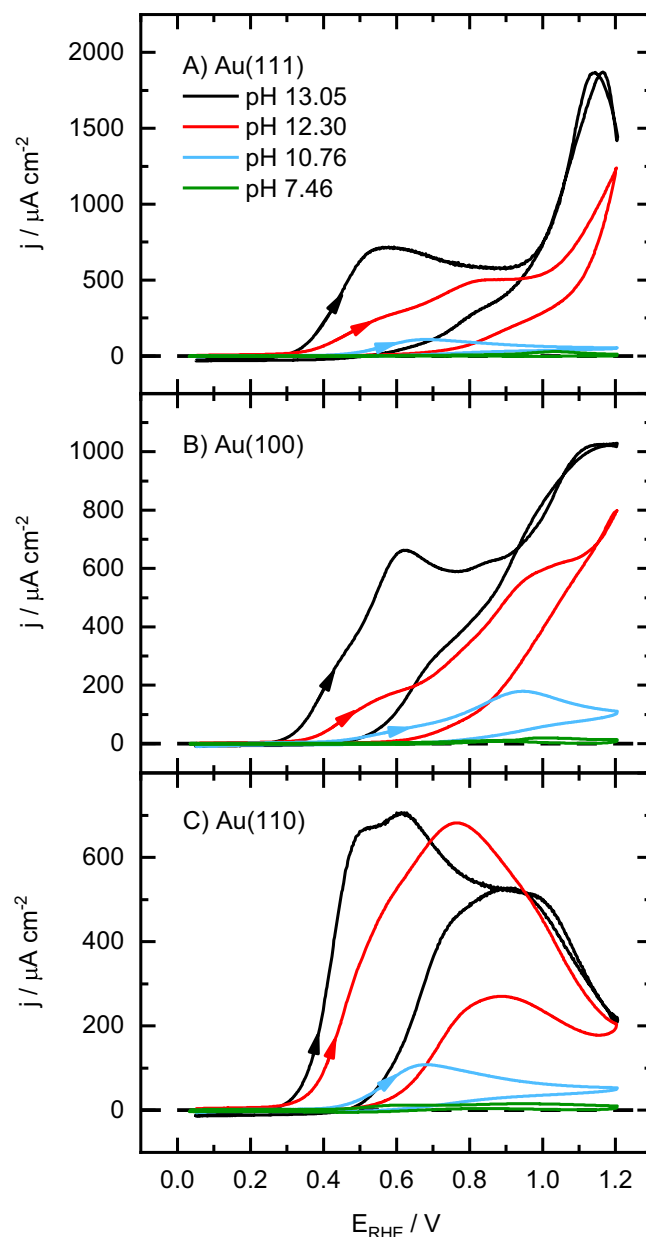


Fig. 6 | Influence of different pH conditions on HMF electrooxidation at Au single-crystal electrodes. Voltammetric profiles for the oxidation of 3.5 mM HMF on (A) Au(111), (B) Au(100), and (C) Au(110) in 0.1 M NaOH ($\text{pH } 13.05 \pm 0.03$), 0.01 M NaOH + 0.09 M NaClO_4 ($\text{pH } 12.30 \pm 0.03$), 0.001 M NaOH + 0.099 M NaClO_4 ($\text{pH } 10.76 \pm 0.02$), and 0.0086 M NaH_2PO_4 + 0.03 M Na_2HPO_4 ($\text{pH } 7.46 \pm 0.03$). Scan rate: 50 mV s^{-1} . Source data are provided as a Source Data file.

conditions, the gem-diol, which has a pK_a of 12.82, can further deprotonate to produce the gem-diolate species. These transformations occur preferentially over the direct formation of the alkoxide due to the higher reactivity and stabilization of the intermediate hydroxyl groups involved in the gem-diol formation. This stabilization makes the gem-diol and gem-diolate species prevalent in alkaline conditions compared to the alkoxide³⁴.

To understand the role of these equilibria, experiments at different pH values were conducted (Fig. 6). As can be seen, a significant oxidation current dependence on the pH is observed. Currents diminish as the pH is made more acidic. Moreover, the pH changes affect differently to the two main processes that appear in the voltammetric profile. For the process at low potentials on the Au(111) and Au(100) surfaces, the onset potential shifts to higher values and

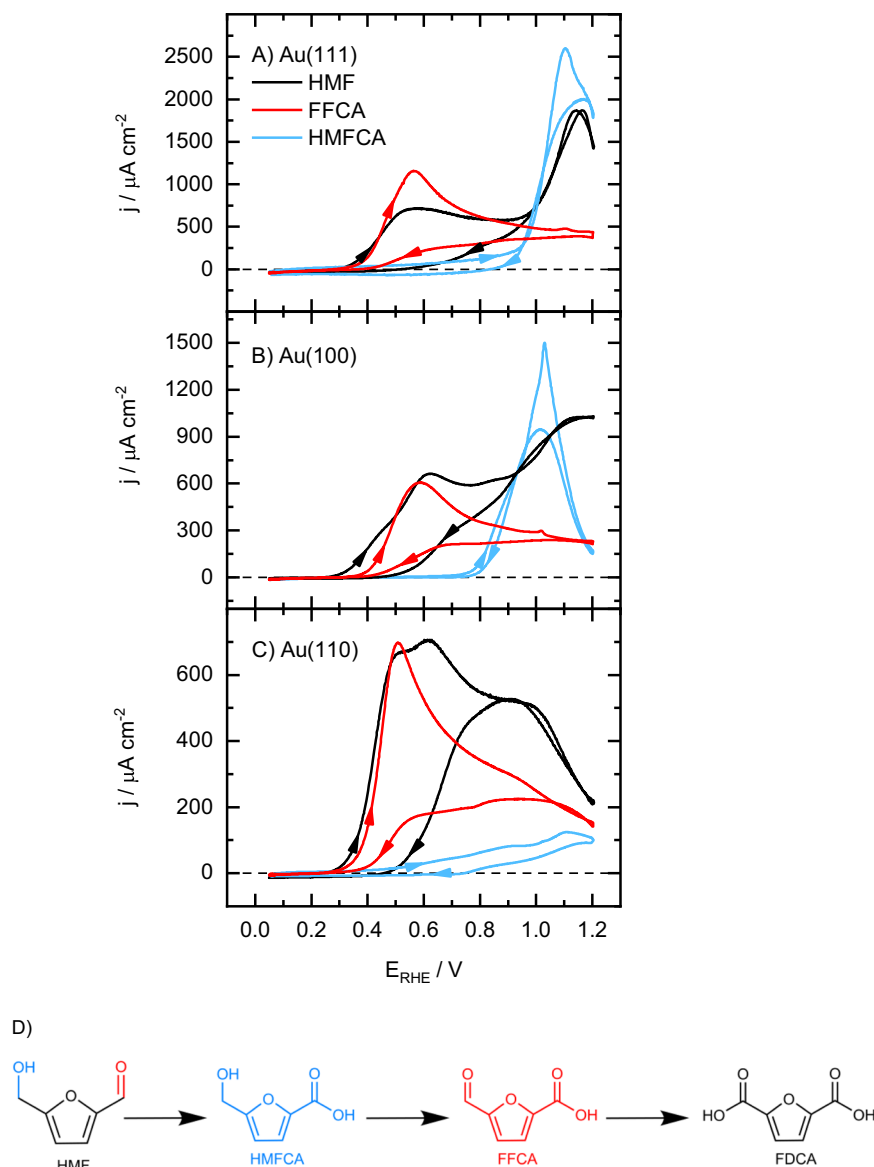


Fig. 7 | Comparative voltammetric evaluation of the HMF oxidation pathway on Au single-crystal electrodes. Voltammetric profiles of the (A) Au(111), (B) Au(100), and (C) Au(110) electrodes in solutions containing 3.5 mM HMF, 3.5 mM HMFCa, and 3.5 mM FFCA in 0.1 M NaOH. Scan rate: 50 mV·s⁻¹. Below, the schematic (D)

illustrates the stepwise oxidation pathway, showing the conversion of HMF to HMFCa, HMFCa to FFCA, and FFCA to FDCA. The hydroxyl group and HMFCa are highlighted in red, while the aldehyde group and FFCA are highlighted in blue. Source data are provided as a Source Data file.

currents diminish significantly when decreasing the pH value, even for pH=12. On the other hand, the process at high potentials is less affected at this pH value. For the Au(110) electrode, the observed changes are smaller. In all cases, currents are almost negligible at pH values below 11. Thus, it can be proposed that the gem-diol equilibria are involved in the activation of the HMF oxidation reaction on gold.

Electrochemical behavior of possible HMF intermediate species

Previous investigations have elucidated that the oxidation pathway of HMF on gold surfaces proceeds via HMFCa as an intermediate^{6,11,18,35}, with the possible formation of FFCA. Furthermore, the formation of DFF was not observed. In order to determine the role of these species as possible intermediates, their electrochemical behavior was studied on the Au single-crystal electrodes (Figs. 7 and S6). First, the oxidation of FDCA was studied (Fig. S8). As can be seen, the profiles are almost identical to those obtained in the absence of FDCA, which implies that if FDCA is produced from the oxidation of HMF, this would

be the final product, because its further oxidation does not take place in the explored potential range. Confirming this through HPLC would have been ideal, but the small area of our electrodes did not allow us to quantify the products. Moreover, significant currents are measured for the oxidation of the two possible intermediates, HMFCa and FFCA, as shown in Fig. 7. The electrochemical oxidation of HMFCa involves the conversion of a hydroxyl group to an aldehyde yielding FFCA. The further oxidation of FFCA entails the conversion of an aldehyde group to a carboxylic acid, producing FDCA as the final product since the breaking of the ring or the bonds of the carboxylic groups for this latter compound does not take place even at high potentials (Fig. S8).

As shown in Fig. 7, the oxidation of the aldehyde group in FFCA to the carboxylic acid has the typical profile of an irreversible process controlled by diffusion, in which, after the peak at ca. 0.50 V, currents in the voltammetric profiles show a slow decay, due to the increasing diffusion layer. The profile closely resembles that obtained for the first

process of HMF oxidation, as can be seen from the comparison of the profiles for the oxidation of both species in Fig. 7. To verify the diffusion control, it would have been desirable to conduct further investigations using the hanging meniscus rotating disk electrode (HMRDE) method. However, due to the ductility of gold, the gold wire holding the single-crystal bead bends at relatively low rotation rates, preventing meaningful measurements. It should be noted that currents for the FFCA are somehow larger than those measured for HMF up to 0.80 V. An additional difference is that unlike the behavior observed with HMF, the profile for FFCA oxidation exhibits a small peak indicative of the removal of the reconstruction of Au(111) and Au(100) surfaces. This observation suggests differences in how FFCA and HMF interact with electrode surfaces. For the HMF oxidation reaction, the current exhibits minimal variation up to approximately 0.90 V, beyond which a further increase in current is noted at higher potentials. This current increase coincides with the onset potential for HMFOA oxidation. The oxidation of HMFOA involves the oxidation of the alcoholic group, first to an aldehyde group and eventually to a carboxylic group. This onset potential is very similar to that observed for the oxidation of much simpler alcohols, such as ethanol²⁶.

With all these data on mind, the voltammetric profile of the HMF oxidation reaction can be understood. In the positive scan direction, between 0.30 and 0.80 V (where the first electrochemical process is observed), the aldehyde group in HMF is oxidized to a carboxylic group (which, at this pH, will deprotonate giving rise to a carboxylate), to yield HMFOA. For the studied concentration, this process is controlled by the diffusion of HMF from the bulk solution to the electrode surface, similarly to what is observed with FFCA. Beyond 0.90 V, HMFOA is further oxidized to FFCA. At these potentials, FFCA is readily oxidized to FDCA. Thus, between 0.90 and 1.20 V, HMF is oxidized to FDCA through the formation of HMFOA and FFCA.

The different structure sensitivity of the intermediates also serves to explain the differences observed previously for the two processes in the oxidation of HMF. For that, the values of the current density maxima in the positive scan direction at 0.45 and 1.15 V are plotted for the different surfaces (Fig. 8). As mentioned before, these plots show that the reactivity for the oxidation of the aldehyde group in HMF to the carboxylic acid is catalyzed by the presence of steps or (110) sites. These results are consistent with a recently published study in which density functional theory (DFT) was employed to investigate the facet dependence of HMF oxidation³⁶. In that study, it was determined that the Au(110) surface does not present an energy barrier for the activation of the C–H bond in the gem-diolate ion intermediate, thereby justifying the higher catalytic activity of Au(110) for the oxidation of HMF to HMFOA. This finding aligns with our results obtained for Au(110) and the high-index single-crystals. On the other hand, the current at 1.15 V, which corresponds to the oxidation of the alcoholic group follows the opposite trend. It is noteworthy that the oxidation of the alcoholic group, as evidenced by the HMFOA oxidation voltammograms, is not favored on Au(110), despite of being the least densely packed basal plane and generally anticipated to be the most reactive surface. However, these findings indicate that less densely packed surfaces, including Au(110), Au(311), Au(331), and Au(210), exhibit reduced activity within the potential range where alcohol group oxidation initiates, in contrast to the significant activity observed on Au(111) and Au(100). This counterintuitive result can be attributed to several factors. It has been suggested that HMF adsorbs onto the electrode surface via its furan ring¹⁴. First of all, the less effective adsorption of HMFOA on Au(110), whose open structure may not provide the optimal configuration for stable adsorption, likely contributes significantly to a low surface concentration and subsequently a poor oxidation. Additionally, the competition for adsorption sites between HMFOA and OH[−] on Au(110) could impede the oxidation process, as OH[−] might occupy the active sites preferentially. Furthermore, the kinetic barriers for the oxidation of the alcohol group in

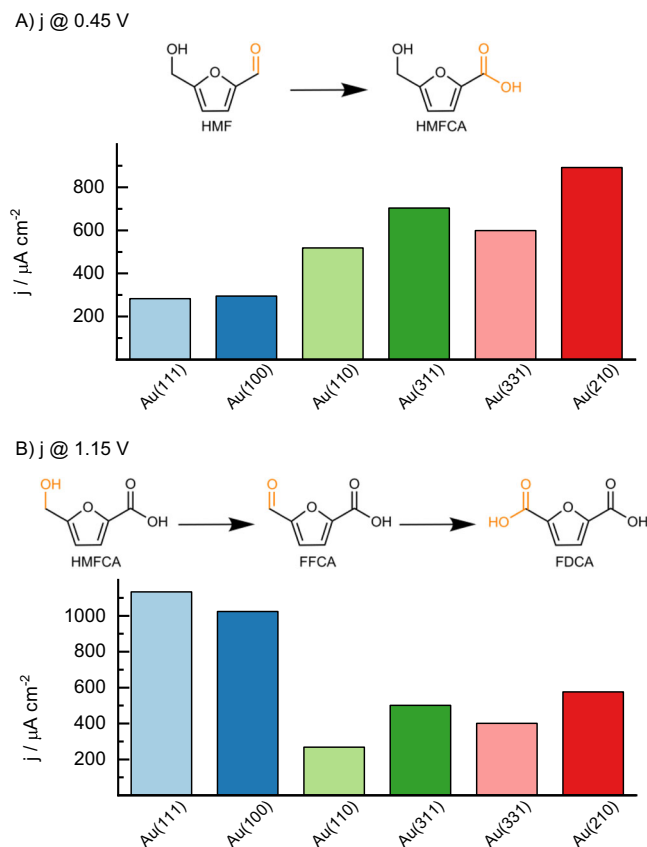


Fig. 8 | Comparative current density analysis at key potentials during HMF electrooxidation on Au single-crystal electrodes. Current density on the different gold single-crystals at 0.45 V (A) and 1.15 V (B) during the positive scan direction of cyclic voltammetry experiments in 3.5 mM HMF + 0.1 M NaOH. Scan rate: 50 mV s^{−1}.

HMFOA might be higher on Au(110), making the reaction less favorable. Considering that the oxidation of small alcohols is typically favored on less densely packed surfaces and the oxidation of the HMF alcoholic group is preferred on more densely packed and planar surfaces, it is inferred that there is a specific interaction between the surface and the π -electrons of the aromatic ring. This π -electron interaction likely enhances the adsorption and stabilization of HMFOA on the planar surfaces of Au(111) and Au(100), facilitating the oxidation reaction, while hindering it on defect-rich surfaces such as Au(110).

In situ IRRAS measurements

In situ infrared spectroscopy studies were performed to elucidate the interaction of HMF with the gold surfaces and the possible oxidation reaction pathways. Figure 9 presents representative IRRAS spectra obtained with p-polarized light for Au(111) and Au(100) electrodes during a linear voltammetric scan in a solution containing 3.5 mM HMF and 0.1 M NaOH. To further investigate the eventual adsorption of HMF and related species, additional experiments were performed with s-polarized light. Given the similarity of the molecules studied and the proximity of the IR vibrational bands, ATR spectra of 0.1 M NaOH solutions containing HMF or potential oxidation products formed during its electrochemical oxidation were registered (Fig. S9). The frequencies and tentative assignments of the main bands in the obtained IRRAS and ATR spectra are summarized in Table 1.

In the in situ IRRAS spectra obtained with p-polarized light for the Au(111) and Au(100) electrodes (Fig. 9), several bands can be identified depending on the electrode potential. These features are essentially the same as those observed in the spectra collected for the Au(111)

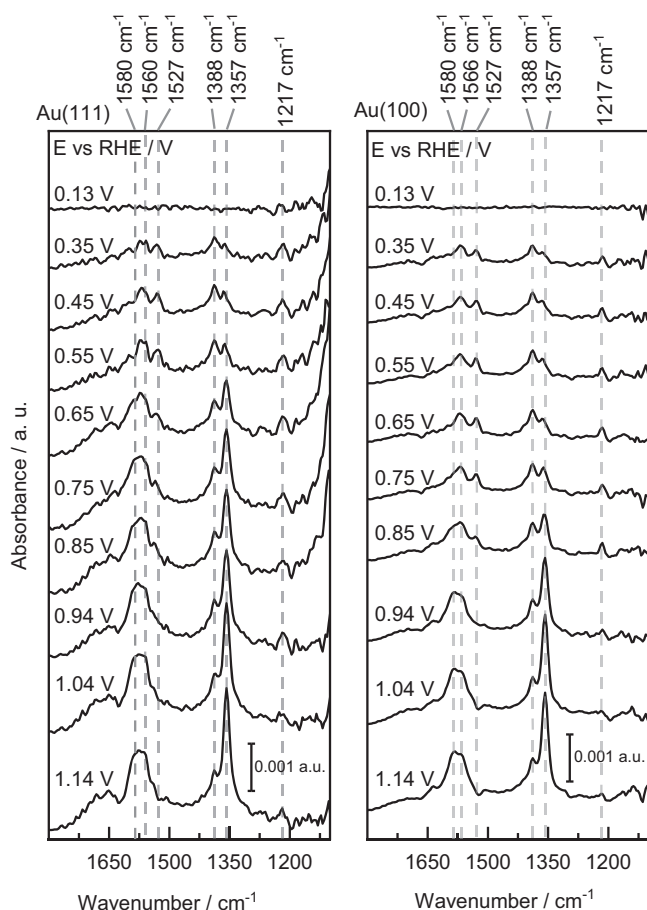


Fig. 9 | In situ IRRA monitoring of HMF electrooxidation on Au(111) and Au(100) single-crystal electrodes. IRRA spectra obtained during a linear potential scan for Au(111) and Au(100) electrodes in a solution containing 3.5 mM HMF and 0.1 M NaOH using p-polarized light. The reference spectra were taken at 0.06 V. Source data are provided as a Source Data file.

electrode with s-polarized light (Fig. S10). For potentials above 0.30 V and coinciding with the onset potential for the HMF oxidation observed in the voltammetry experiments, positive bands in the spectra appear, indicating the formation of some intermediates and/or reaction products. The bands at 1566 cm^{-1} , 1527 cm^{-1} , 1388 cm^{-1} , and 1357 cm^{-1} align with those identified in the ATR spectrum of HMFA (see Fig S7 and Table 1). The band at 1527 cm^{-1} could correspond to the asymmetric OCO stretch, whereas bands at 1388 cm^{-1} and 1357 cm^{-1} are related to the symmetric OCO stretch^{26,35–37}. Roman et al.²⁶ related, on the bases of DFT calculations, some bands below 1400 cm^{-1} in the ATR-SEIRA spectra collected during furfural oxidation to furoate adspecies with an upright conformation binding via a deprotonated carboxylate group²⁶. The same authors proposed that a feature at ca. at 1566 cm^{-1} correlates with ring stretches for this adsorbed species²⁶. Thus, it could be concluded from the spectra in Fig. 9 that HMFA is formed^{26,35–37} during the oxidation of HMF on both Au(111) and Au(100) electrodes at the onset potential. The absence of a band at 1656 cm^{-1} in the IRRA spectra for both electrodes suggests that DFF is not formed during the oxidation process. This finding is consistent with the results obtained from cyclic voltammetry, which indicate the preferential oxidation of the aldehyde group in HMF over the alcohol group during the first process. The non-formation of DFF supports the notion that the aldehyde group oxidizes more readily under the given experimental conditions.

Figure 9 shows that the intensity of the aforementioned bands increases as the potential increases. However, a clear change in the

Table 1 | Identification of different species and band adsorption observed in the IRRA and ATR-IR spectra of HMF related species dissolved in 0.1 M NaOH

$\nu_{\text{IRRAS}} / \text{cm}^{-1}$	$\nu_{\text{ATR}} / \text{cm}^{-1}$	Species	Assignments
$E < 0.80 \text{ V}$	$E > 0.80 \text{ V}$		
1357	1353	FFCA	Symmetric OCO stretching of deprotonated carboxylate group ^{7,27,37,41}
	1357	FDCA	
	1364	HMFA	
1388	1388	HMFA	
	1407	FFCA	
1527	1527	HMFA	Asymmetric OCO stretching of deprotonated carboxylate ^{7,27,37}
1566	1566	HMFA	Ring stretches ²⁷
	1579	FDCA	
1580	1593	FFCA	
	1652	HMFA	Gem-diol vibration ³⁷
	1656	DFF	
	1660	HMF	
	1670	FFCA	

relative intensities of the bands and the appearance of new bands is observed above 0.65 and 0.75 V, for the Au(111) and Au(100) surfaces, respectively. Note that the onset potential for these changes coincides with that observed in the voltammetric profile for the second process (Fig. 2). This coincidence indicates the formation of new species that could be identified from the spectroscopic data. In this way, the increasing intensity of a band at 1357 cm^{-1} with respect to that of the band at 1388 cm^{-1} , which is the main feature in this spectral region for HMFA species, suggests the formation of either FFCA or FDCA on both electrodes upon HMFA oxidation. In this sense, the band at 1527 cm^{-1} , which is also characteristic of HMFA, has disappeared, suggesting that HMFA has been completely oxidized. Regarding the nature of the formed species, it can be pointed out that the spectra at 1.14 V are very close to that obtained for FDCA. Besides, the broadening of the band near 1566 cm^{-1} (with a marked shoulder at ca. 1580 cm^{-1}), together with the absence of a band at 1275 cm^{-1} , characteristic of FFCA, seem to indicate that FDCA is the prevailing oxidation product. Nevertheless, it should be noted that the formation of some traces of FFCA cannot be discarded, because the characteristic bands would be masked by those related to the formation of FDCA or the consumption of HMF. All these results indicate that, in the potential region between 0.80 and 1.20 V, the complete oxidation of HMF to FDCA is possible with a high current efficiency. Also, deduced from the voltammetric behavior of HMF and the different intermediates, the oxidation of the aldehyde group is significantly easier than that of the alcoholic group²⁶.

As stated above, the in situ experiment carried out with p- and s-polarizations yielded very similar spectra. Considering the surface selection rule and the external reflection configuration used, with the infrared beam probing both the electrode surface and the thin solution layer between the electrode and the infrared window, it has to be concluded that all the observed features have necessarily contributions from dissolved species. This result is consistent with the potential-independent band frequencies of all the observed bands in Fig. 9. Note also that these features match quite well with the operando ATR-IR spectra reported for HMF oxidation on nickel boride electrodes⁷. Due to the internal reflection configuration used in this latter work, with the working electrode surface placed close to a Ge reflecting window (Otto's configuration), one can expect that the bands observed under these conditions

corresponds only to dissolved species. In any case, we cannot preclude from our results the existence of some adsorbed species coming from HMF or its oxidation products. More surface-specific experiments, such as ATR-SEIRAS, should be carried out to detect these adsorbates. The limited stability in strongly alkaline solutions of the silicon window typically used in these experiments is a strong drawback to be solved³⁸.

The results presented in this study emphasize the significant influence of gold electrode surface orientation on the electrochemical oxidation of HMF in alkaline media. The experiments conducted on Au(111), Au(100), and Au(110) surfaces have revealed differences in catalytic activity and product selectivity. Notably, the Au(111) and Au(100) surfaces exhibited a higher tendency towards the complete oxidation of HMF to FDCA. In contrast, the Au(110) surface was more selective towards the formation of HMFA, an intermediate product. Additionally, the stepped surfaces provided additional insights into how specific atomic arrangements affect the oxidation process. The oxidation of HMF on these surfaces, which simulate real catalytic conditions, occurs at lower potentials than on the three basal planes. These findings highlight the role of the crystallographic structure and surface defects of the gold surfaces in modulating reaction pathways and intermediate formation. The use of in situ IRRAS further confirmed the presence of different intermediate species formed during the oxidation process. Moreover, varying the upper potential limit during cyclic voltammetry revealed significant effects on the oxidation process. At potentials lower than 0.90 V, HMFA is formed in a process controlled by kinetics and diffusion, whereas at higher potentials this intermediate is further oxidized to FDCA. The experiments also showed that the effect of pH is different for the two processes. Lowering the pH, i.e., lowering the amount of gem-diol, notably hinders the oxidation of HMF to HMFA on Au(111) and Au(100), whereas the oxidation at $E > 0.90$ V is less affected.

In conclusion, this study provides a comprehensive understanding of the relationship between surface structure and catalytic activity in the electrochemical oxidation of HMF on gold electrodes. The findings not only advance the understanding of structure-activity relationships but also provide a strong foundation for optimizing catalyst design for sustainable energy applications, particularly in the conversion of biomass-derived molecules into high-value chemicals.

Methods

Au single-crystal electrodes were prepared using Clavilier's method^{39,40}. A 0.5 mm diameter gold wire (99.999 %) was melted using a compact propane-oxygen torch and allowed to cool gradually, forming a single crystal bead. This bead was mounted in a four-cycle goniometer on an optical bench and was aligned accurately via laser beam reflections. After orientation, the bead was cut and polished with diamond paste to achieve a mirror finish.

The electrochemical measurements were conducted employing a HydroFlex reversible hydrogen reference electrode (RHE) for solutions at pH values of 1, 13, and 12, and an Ag/AgCl_{sat} electrode for the pH 10 and pH 7 solutions. pH values were measured twice before the experiments and twice again afterwards, and the reported uncertainty refers to the standard deviation of these measured values. Calibration of the reference electrode is ensured by recording a blank measurement with Au single-crystals, since the relevant peak potentials are well established. To facilitate comparison, all electrode potentials are referred to the RHE scale. The potential is not iR corrected. While similar results can be achieved using a glassy carbon counter electrode or an H-type cell, we selected a single-compartment cell equipped with a gold wire counter electrode. Unlike glassy carbon, the gold wire can be flame-annealed, thereby minimizing contamination and ensuring a cleaner surface. For this

reason, it was chosen as the counter electrode. Moreover, the single-compartment configuration is easier to clean than an H-cell, a factor of crucial importance when working with single-crystal electrodes. Therefore, two single-compartment glass cells were used. During the experiments, one cell was used for 0.1 M NaOH, and the other for 0.1 M NaOH + 3.5 mM HMF. Each day, the cells were thoroughly washed and used with either solution, as both setups yielded consistent results. Before the experiments, the gold single-crystal electrodes were flame annealed to reestablish the surface structure and remove any adsorbed impurities. Then, they were quenched and protected with a water droplet. The experimental solutions were composed of 5-hydroxymethylfurfural ($\geq 99\%$, Sigma-Aldrich), sodium hydroxide monohydrate (Merck, Suprapur®, 99.99%), disodium hydrogen phosphate (Merck, anhydrous, Suprapur®, 99.99%), sodium di-hydrogen phosphate (Merck, anhydrous, Suprapur®, 99.99%), sodium perchlorate (Alfa Aesar, anhydrous, ACS, 98.0–102.0%) and ultrapure water (18.2 MΩ cm, TOC 50 ppb max). All solutions were deoxygenated with argon (Ar N50, Air Liquide). Voltammetric experiments were performed at room temperature of approximately 25 °C, using an eDAQ 161 potentiostat connected with an EG&G PARC 175 wave signal generator and an eDAQ 401 recorder.

IRRAS experiments were conducted using a Nicolet iS50 (Thermo Scientific) FTIR spectrometer, which was equipped with a narrow-band DC-coupled MCT-A detector. The spectroelectrochemical cell featured a prismatic CaF₂ window bevelled at an angle of 60°. These experiments were performed at room temperature of approximately 25 °C. A RHE served as the reference electrode, while a gold wire was used as the counter electrode. The IR spectra were obtained averaging 114 interferograms, which were collected with either s- or p-polarized light with a spectral resolution of 8 cm⁻¹. The interferograms were obtained during a positive potential sweep at 2 mV s⁻¹ between 0.05 and 1.20 V. Thus, the resulting single beam spectra corresponds to a time window of 10 s (i. e., a 20 mV interval). The spectra are presented as the ratio $-\log(R/R_0)$, where R and R_0 represent the reflectance values corresponding to the single beam spectra recorded at the sample and reference potentials, respectively. The reference spectra were acquired at 0.06 V. Positive bands in the spectra indicate species formed or whose concentration has increased at the sampling potential relative to the reference potential, whereas negative bands indicate a decrease in the species concentration. Additionally, ATR-IR experiments were conducted using a ZnSe window bevelled at 45° to obtain the spectra for alkaline solutions of HMF and its derivatives. These spectra are referenced to a single beam spectrum collected with a 0.1 M NaOH solution.

Data availability

All data presented in the main article and Supplementary Information are available from the authors upon request. The data of Figs. 2–4, 6, 7, 9, S1 and S3–S10 used in this study are available in the figshare database under accession code <https://doi.org/10.6084/m9.figshare.28477124>.

References

1. Yang, Y. & Mu, T. Electrochemical oxidation of biomass derived 5-hydroxymethylfurfural (HMF): pathway, mechanism, catalysts and coupling reactions. *Green. Chem.* **23**, 4228–4254 (2021).
2. Harhues, T. et al. Integrated biphasic electrochemical oxidation of Hydroxymethylfurfural to 2,5-Furandicarboxylic Acid. *ACS Sustain. Chem. Eng.* **11**, 8413–8419 (2023).
3. Cai, M. et al. Nickel(ii)-modified covalent-organic framework film for electrocatalytic oxidation of 5-hydroxymethylfurfural (HMF). *Chem. Commun.* **56**, 14361–14364 (2020).
4. Feng, Y. et al. Metal sulfide enhanced metal-organic framework nanoarrays for electrocatalytic oxidation of 5-hydroxymethylfurfural to 2,5-furandicarboxylic acid. *J. Mater. Chem. A Mater.* **11**, 6375–6383 (2023).

5. Carvajal, D. et al. Electrochemical valorization of HMF using Ni/Graphite electrodes. *Mater. Chem. Phys.* **311**, 128510 (2024).
6. Chadderton, D. J. et al. Electrocatalytic oxidation of 5-hydroxymethylfurfural to 2,5-furandicarboxylic acid on supported Au and Pd bimetallic nanoparticles. *Green. Chem.* **16**, 3778–3786 (2014).
7. Barwe, S. et al. Electrocatalytic oxidation of 5-(Hydroxymethyl)furfural using high-surface-area nickel boride. *Angew. Chem. Int. Ed.* **57**, 11460–11464 (2018).
8. Zhang, J. et al. Boosting HMF oxidation performance via decorating ultrathin nickel hydroxide nanosheets with amorphous copper hydroxide islands. *J. Mater. Chem. A Mater.* **9**, 9685–9691 (2021).
9. Fan, Z. et al. Self-Reconstruction of sulfate-terminated copper oxide nanorods for efficient and stable 5-hydroxymethylfurfural electro-oxidation. *Nano Lett.* <https://doi.org/10.1021/acs.nanolett.3c03949>.
10. Megías-Sayago, C. et al. Effect of Gold Particles Size over Au/C catalyst selectivity in HMF oxidation reaction. *ChemCatChem* **12**, 1177–1183 (2020).
11. Davis, S. E. et al. On the mechanism of selective oxidation of 5-hydroxymethylfurfural to 2,5-furandicarboxylic acid over supported Pt and Au catalysts. *Green. Chem.* **14**, 143–147 (2012).
12. Latsuzbaia, R. et al. Continuous electrochemical oxidation of biomass derived 5-(hydroxymethyl)furfural into 2,5-furandicarboxylic acid. *J. Appl. Electrochem.* **48**, 611–626 (2018).
13. Rodriguez, P. & Koper, M. T. M. Electrocatalysis on gold. *Phys. Chem. Chem. Phys.* **16**, 13583–13594 (2014).
14. Sobota, L. et al. Impact of the electrochemically inert furan ring on the oxidation of the alcohol and aldehyde functional group of 5-Hydroxymethylfurfural (HMF). *ChemElectroChem* **11**, e202300151 (2023).
15. Fu, G. et al. Capturing critical gem-diol intermediates and hydride transfer for anodic hydrogen production from 5-hydroxymethylfurfural. *Nat. Commun.* **14**, 8395 (2023).
16. Gidi, L. et al. Recent progress, trends, and new challenges in the electrochemical production of green hydrogen coupled to selective electrooxidation of 5-hydroxymethylfurfural (HMF). *RSC Adv.* **13**, 28307–28336 (2023).
17. Zhang, R. et al. Boosting hydrogen evolution via anodic oxidation of 5-hydroxymethylfurfural in anion exchange membrane electrolyzer over a metallic heterostructure. *Mater Today. Nano* **23**, 100373 (2023).
18. Vuyyuru, K. R. & Strasser, P. Oxidation of biomass derived 5-hydroxymethylfurfural using heterogeneous and electrochemical catalysis. *Catal. Today* **195**, 144–154 (2012).
19. Krebs, M. L. et al. Stabilization of alkaline 5-HMF electrolytes via Cannizzaro reaction for the electrochemical oxidation to FDCA. *Green. Chem.* **25**, 1797–1802 (2023).
20. Hamelin, A. et al. Cyclic voltammetric characterization of oriented monocrystalline gold surfaces in aqueous alkaline solution. *J. Electroanal. Chem. Interfacial Electrochem.* **295**, 291–300 (1990).
21. Batina, N. et al. The surface structure of flame-annealed Au(100) in aqueous solution: an STM study. *J. Electroanal. Chem.* **370**, 87–94 (1994).
22. Strbac, S. et al. Electrochemical indication of surface reconstruction of (100), (311) and (111) gold faces in alkaline solutions. *J. Electroanal. Chem.* **362**, 47–53 (1993).
23. Gallagher, M. E. et al. Structure sensitivity of CO oxidation on gold single crystal surfaces in alkaline solution: surface X-ray scattering and rotating disk measurements. *Surf. Sci.* **582**, 215–226 (2005).
24. Kolb, D. M. Reconstruction phenomena at metal-electrolyte interfaces. *Prog. Surf. Sci.* **51**, 109–173 (1996).
25. Skotuda, P. The extension of the stability range of the reconstructed Au(111) surface by propanal. *Z. f.ür. Physikalische Chem.* **219**, 463–466 (2005).
26. Beyhan, S. et al. Electrochemical and in situ FTIR studies of ethanol adsorption and oxidation on gold single crystal electrodes in alkaline media. *J. Electroanal. Chem.* **707**, 89–94 (2013).
27. Román, A. M. et al. Electro-oxidation of furfural on gold is limited by furoate self-assembly. *J. Catal.* **391**, 327–335 (2020).
28. Climent, V. et al. Potential of zero total charge of platinum single crystals: a local approach to stepped surfaces vicinal to Pt(111). *Russian J. Electrochem.* **42**, 1145–1160 (2006).
29. Iannelli, A. & Lipkowski, J. Potential-controlled coordination of coumarin to an Au(210) electrode surface. *J. Phys. Org. Chem.* **16**, 675–681 (2003).
30. Hamelin, A. & Lecoeur, J. The orientation dependence of zero charge potentials and surface energies of gold crystal faces. *Surf. Sci.* **57**, 771–774 (1976).
31. Kwon, Y. et al. Electrocatalytic oxidation of alcohols on gold in alkaline media: base or gold catalysis? *J. Am. Chem. Soc.* **133**, 6914–6917 (2011).
32. Zope, B. N. et al. Reactivity of the Gold/Water interface during selective oxidation catalysis. *Science* **330**, 74–78 (2010).
33. Bondue, C. J. et al. Electrochemical aldehyde oxidation at gold electrodes: gem-Diol, non-Hydrated Aldehyde, and diolate as electroactive species. *ChemSusChem* **16**, e202300685 (2023).
34. Vollhardt, K. P. C. & Schore, N. E. *Organic chemistry: structure and function* (W. H. Freeman and Company, 1997).
35. Davis, S. E. et al. Oxidation of 5-hydroxymethylfurfural over supported Pt, Pd and Au catalysts. *Catal. Today* **160**, 55–60 (2011).
36. Qin, Q. et al. Unveiling the gold facet effect in selective oxidation of 5-Hydroxymethylfurfural and hydrogen production. *Nano Lett.* <https://doi.org/10.1021/acs.nanolett.4c04786> (2024).
37. Martínez-Hincapié, R. et al. Weakening the C-C bond: on the behavior of glyoxylic acid on Pt(111) and its vicinal surfaces. *J. Electroanal. Chem.* **779**, 75–85 (2016).
38. Zhang, W.-Y. et al. Atomic layer deposition of TiO₂ on Si window enables in situ ATR-SEIRAS measurements in strong alkaline electrolytes. *Anal. Chem.* **96**, 10111–10115 (2024).
39. Clavilier, J. et al. Electrochemical adsorption behaviour of platinum stepped surfaces in sulphuric acid solutions. *J. Electroanal. Chem. Interfacial Electrochem* **205**, 267–277 (1986).
40. Korzeniewski, C. et al. Electrochemistry at platinum single crystal electrodes. in *electroanalytical chemistry. A Ser. Adv.* **24**, 75–170 (2011).
41. Cuesta, A. et al. Electrooxidation of formic acid on gold: an ATR-SEIRAS study of the role of adsorbed formate. *Catal. Today* **202**, 79–86 (2013).

Acknowledgements

Financial support from the Ministerio de Ciencia, Innovación y Universidades (grant number PID2022-137350NB-I00) is acknowledged. L.C.M. acknowledges support from the predoctoral fellowship awarded by Ministerio de Ciencia, Innovación y Universidades (grant number PREP2022-000182). R.M.A.A. acknowledges the financial support from Ramón y Cajal Fellowship from Ministerio de Ciencia, Innovación y Universidades (grant number RYC2022-038206-I).

Author contributions

E.H., R.M.A.A., and L.C.M. planned the experiments. L.C.M. conducted the electrochemical experiments. A.R. assisted with the setup of the infrared spectroscopy experiments. A.R. and L.C.M. conducted the infrared spectroscopy experiments. L.C.M. wrote the initial version of the manuscript and supporting information. All authors discussed the results and provided feedback on the manuscript at every stage.

Competing interests

The authors declare no competing interest.

Additional information

Supplementary information The online version contains supplementary material available at <https://doi.org/10.1038/s41467-025-58696-4>.

Correspondence and requests for materials should be addressed to Rosa M. Arán-Ais.

Peer review information *Nature Communications* thanks Wooyul Kim, Tiancheng Mu, and the other, anonymous, reviewer for their contribution to the peer review of this work. A peer review file is available.

Reprints and permissions information is available at <http://www.nature.com/reprints>

Publisher's note Springer Nature remains neutral with regard to jurisdictional claims in published maps and institutional affiliations.

Open Access This article is licensed under a Creative Commons Attribution-NonCommercial-NoDerivatives 4.0 International License, which permits any non-commercial use, sharing, distribution and reproduction in any medium or format, as long as you give appropriate credit to the original author(s) and the source, provide a link to the Creative Commons licence, and indicate if you modified the licensed material. You do not have permission under this licence to share adapted material derived from this article or parts of it. The images or other third party material in this article are included in the article's Creative Commons licence, unless indicated otherwise in a credit line to the material. If material is not included in the article's Creative Commons licence and your intended use is not permitted by statutory regulation or exceeds the permitted use, you will need to obtain permission directly from the copyright holder. To view a copy of this licence, visit <http://creativecommons.org/licenses/by-nc-nd/4.0/>.

© The Author(s) 2025